

Article

Investigating the Potential of Greener-Porous Graphene for the Treatment of Organic Pollutants in Wastewater

Bhavya Joshi *, Ahmed M. E. Khalil , Shaowei Zhang * and Fayyaz A. Memon *

Department of Engineering, University of Exeter, Exeter EX4 4QF, UK; a.a.khalil@exeter.ac.uk

* Correspondence: bj300@exeter.ac.uk (B.J.); s.zhang@exeter.ac.uk (S.Z.); f.a.memon@exeter.ac.uk (F.A.M.)

Abstract: Pharmaceuticals have emerged as a new class of ecological pollutants and have majorly contributed to harmful effects on the environment and human health. The presence of these pharmaceuticals in wastewater treatment plants, ground, and seawater has been reported widely. Organic dyes and other organic contaminants which are being considered as emerging contaminants are now in the race among the top organic pollutants that need effective treatment. Removal of these contaminants via green adsorbents has become an essential requirement towards a green and cleaner environment. Herein, we report the efficacy of the novel greener porous graphene obtained via the near-green synthesis method as an adsorbent material for treating seven organic pollutants: Methyl orange, Methyl red, Rhodamine-B, Ciprofloxacin, Atenolol, Ibuprofen, and Carbamazepine. Batch tests were conducted to investigate the effect of adsorption time and varying adsorbent dosages. The obtained greener porous graphene showed fast kinetics, which was determined to be guided by pseudo second-order kinetics and the maximum pollutant removal efficiency (>80%) was seen at a high adsorbent dosage (2 mL injected from a 5 g/L solution). Furthermore, the nonlinear adsorption modeling confirmed that the greener porous graphene followed the Langmuir model for the dye rhodamine-B sorption and the Freundlich model for all the other six contaminants. This greener porous graphene can be considered an effective adsorbent for the removal of organic pollutants in wastewater.

Keywords: greener porous graphene; near-green synthesis; emerging contaminants; organic dyes; Akaike information criterion; adsorption; water treatment



Citation: Joshi, B.; Khalil, A.M.E.; Zhang, S.; Memon, F.A. Investigating the Potential of Greener-Porous Graphene for the Treatment of Organic Pollutants in Wastewater. *C* **2023**, *9*, 97. <https://doi.org/10.3390/c9040097>

Academic Editors: Jorge Bedia and Carolina Belver

Received: 25 August 2023

Revised: 25 September 2023

Accepted: 30 September 2023

Published: 7 October 2023



Copyright: © 2023 by the authors. Licensee MDPI, Basel, Switzerland. This article is an open access article distributed under the terms and conditions of the Creative Commons Attribution (CC BY) license (<https://creativecommons.org/licenses/by/4.0/>).

1. Introduction

Two major industries, i.e., medical and textile, have created a socio-economic milestone in human history [1,2]. Textile industries dispose of their effluents at a rapid rate, and their residue in water sources has caused great concern for human as well as aquatic life [3]. The WHO declared that 4000 children die almost every day due to waterborne diseases originating from inefficient water and wastewater treatment [4].

Of these industrial effluent pollutants, organic dyes are carcinogenic to human health and are prominent noxious contaminants for the environment [5]. Organic dyes account for 15% of the world's total dye production, which is disposed of as waste from fabrics and textile industries [6]. Organic dyes such as Methyl orange (MeO), Methyl red (MeR), and rhodamine-B (RD) are frequently used dyes in the fabric dyeing process. MeO is a water-soluble azo dye with considerable mutagenic properties. The presence of this dye inside the human body can cause serious diseases, such as intestinal cancer [7]. Deterioration in kidneys, liver, lungs, or even nervous systems are all resultant effects of the presence of dyes in the body. MeR is an anionic azo dye that irritates the eye, skin, and gut when ingested [8]. On the other hand, RD is a cationic azo dye that comes with harmful effects, such as dermatitis (skin irritation) and skin cancer [9]. Therefore, these dyes must be treated effectively instead of being disposed of in water bodies.

Pharmaceuticals have increased human quality of life and have helped us fight dangerous diseases. However, their frequent presence in water sources through several means is now a growing concern and they are viewed as ‘emerging contaminants (ECs)’ [10–24]. Due to their considerable presence in the environment, they are often referred to as ‘pseudo persistent’ contaminants [11,25–28]. Groundwater and surface water both contain some pharmaceutical remnants with concentrations nearly less than 100 ng/L, while treated water contains these contaminants at concentrations below 50 ng/L [29]. These levels are soaring across the world, daily, and according to the authors of [30], a very high concentration of pharmaceuticals is present in African and European waters.

Pharmaceuticals commonly found in UK waters are Atenolol (AT), Ibuprofen (IBU), Ciprofloxacin (CPF), and Carbamazepine (CB) [31]. AT is described as Beta-blockers (BB), commonly advised for hypertension, heart rhythmic disease, or myocardial infarctions [32,33]. CB is a frequent drug used in treatment lines for epilepsy and prevents human-embryonic cell growth [34,35]. CPF is considered to be among the top ten fluoroquinolone antibiotics for treating bacteria and fighting infections [36,37], and the presence of this organic pollutant in the environment not only creates an ecological imbalance but also leaves long-term effects in the body when more than the prescribed dose is ingested [38]. IBU is an anti-inflammatory drug, used for the treatment of pain, fever, and rheumatic disorders, and is very commonly used in the UK [39]. If not removed efficiently from the wastewater, it has a detrimental effect on human health and the aquatic ecosystem [40]. Therefore, there is an imperative need to treat the water and wastewater (containing these organic pollutants).

Removal of various contaminants through the adsorption process has proven to be the most efficient and cost-effective method [3,40]. Adsorbents of hydrophobic nature have emerged as an effective removal means for both organic and inorganic contaminants [40]. Porous graphene (PG), i.e., a carbon-based material with super-hydrophobicity, has surfaced as an effective adsorbent for the removal of contaminants such as dyes and heavy metals [3]. PG has also been tested against six emerging contaminants, namely atenolol, carbamazepine, ciprofloxacin, diclofenac, gemfibrozil, and ibuprofen, at their trace concentrations and has been shown to have an effective removal efficiency (>99%) at low PG dosages (100 mg/L) [31]. It also showed good recyclability and effective regeneration for up to four cycles [31]. The removal efficiency of these pharmaceuticals was further increased using PG as a filter media in the adsorption column filter tertiary unit [41]. Various composites, such as GNP/BNA (graphene nanoplatelet/Boron Nitride), with a maximum adsorption capacity of 185 mg/g, have proven to be potential candidates for the removal of ciprofloxacin [42].

Synthesis of PG via various methods has also been studied. Graphene oxide (GO) has proven to be the vital precursor to synthesize PG, and the most common chemical technique to obtain GO is the Hummers method [43]. Several green techniques have been incorporated to achieve PG via GO as the common precursor [44–46]. However, all these green methods use GO as a precursor, synthesized from the techniques involving noxious reactants resulting in the release of toxic gases into the environment. Thus, there is an absolute need for greener adsorbent materials.

A recent novel technique was demonstrated, where a greener method was obtained to synthesize a greener PG [47]. The authors [47] reported a high yield of greener GO synthesized by oxidation of graphite via this near-green technique. The successful synthesis of the as-produced bi-layered greener PG was confirmed via various characterization techniques, such as Atomic Force Microscopy, Transmission Electron Microscopy, X-ray diffraction, and Scanning Electron Microscopy. Herein, for the very first time, we report the Brunauer–Emmett–Teller (BET) Specific Surface area of this novel greener PG and investigate its efficacy in removal of seven emerging contaminants (ECs), such as AT, CB, CPF, IBU, MeO, MeR, and RD.

The aim of this study is to understand the potency of this novel greener PG, synthesized via a near-green route [47], for treating emerging contaminants in wastewater.

For the very first time, this study outlined the removal efficacy of greener PG in water treatment applications and proved its potential as a candidate for an adsorbent material. BET measurements for this novel greener adsorbent were also carried out to investigate and compare the surface area of the PG derived commercially from noxious reagents. This research aimed to establish an environmentally friendly PG adsorbent in the field of wastewater/water treatment.

2. Materials and Methods

2.1. Chemical and Adsorbent Preparation

Graphite powder (~20 μm), Sulphuric Acid (H_2SO_4 :95–98% *w/w*), Paraffin Wax, Ethyl cellulose (48.0–49.8% *w/w*), Cyclohexane (anhydrous 95%), MeO, MeR, RD dye, and analytical-grade pharmaceuticals (AT, CPF, CB, and IBU) were directly purchased from Sigma-Aldrich Co. (Poole, UK) and used without further purification. Potassium ferrate was supplied by Skyrun Industrial Co., Ltd., Nanjing, China, High-Tech Industrial Park, Chemical Zone, Zhejiang, China. Commercial reduced graphene oxide (purity > 99% and thickness 5–10 nm) was purchased internationally from Platonic Nanotech Private Ltd., Kachwa Chowk, Mahagama, Dist.-GODDA, Jharkhand, India.

Preparation of greener PG—The material was obtained via near-green synthesis, as reported in ref. [47].

Preparation of commercial PG—Reduced graphene oxide (rGO) was placed overnight at 200 °C in a vacuum oven to obtain commercial PG.

Pharmaceuticals (AT, CPF, CB, and IBU) and organic dyes (MeO, MeR, RD)—Stock solutions were obtained by mixing pharmaceuticals and dyes with the de-ionized water (DW). To avoid the photo-degradation of these prepared stock solutions, airtight containers were used for their storage and were kept in a dark place.

2.2. Analytical Methods

Microstructural Surface Area Characterization

Brunauer–Emmett–Teller (BET) specific surface area (SSA), porosity, pore volume, and pore size of the greener PG were analyzed using a Quantachrome Autosorb-iQ gas area characterization analyzer. After being heated at 200 °C for four hours to flush out impurities lodged in the pores, the sample (greener PG) was cooled in an external bath at –195.8 °C. After that, the nitrogen gas (N_2) was applied, and the total volume and pressure were then measured.

2.3. Batch Tests and Analysis

All seven pollutants were tested in batches under various experimental settings, including contact time and varying greener PG doses. Each test was run three times, and the average result was used to analyze the data.

2.3.1. Effect of the Contact Time and Study of Kinetic Models

Without adjusting the pH of the contaminated solutions, kinetic experiments were conducted for the pollutants with a starting concentration of 10.0 mg/L (stock solution) throughout various time intervals, at room temperature (22 ± 3 °C) (AT, CB, CPF, IBU, MeO, MeR, and RD). Each of these 20 mL contaminant solutions was placed into 50 mL airtight sealed bottles. These contaminant solutions were then given a specific amount of adsorbent (1 mL injected from a suspension of 5 g of greener PG/L). The solutions were then each magnetically stirred for the allotted amounts of time ($t = 5, 10, 15, 20, 40, 80,$ and 120 min). Finally, a 0.2 μm membrane filter was used to instantly filter the samples that were collected at the designated time.

Two kinetic models: pseudo first-order (Equation (1)) and pseudo second-order (Equation (2)) were used to examine the reaction kinetics of the seven tested contaminants removal by greener PG [48]:

$$\frac{dq}{dt} = k_1(Q_e - Q_t) \quad (1)$$

$$\frac{dq}{dt} = k_2(Q_e - Q_t)^2 \quad (2)$$

where Q_e (mg/g) refers to the equilibrium adsorption capacity, Q_t (mg/g) is the adsorption capacity at a specific time 't', and k_1 (1/min) and k_2 (g/mg min) define the pseudo first- and second-order reaction rate constants, respectively.

2.3.2. Effect of the Adsorbent Dosage and Study of Adsorption Isotherms

The effects of injecting different adsorbent dosages such as 0.5, 1, 1.5, 2, 2.5, and 3 mL from a 5 g/L suspension into a specific contaminant concentration (10 mg/L) were investigated in this batch testing. The contaminants with varying adsorbent dosages were placed in a shaker for 24 h, and finally, the supernatants of the samples were collected using a 0.2 μm membrane filter.

Three models—Langmuir, Freundlich, and Temkin—were analyzed to evaluate the modeling of these seven contaminants' sorption onto greener PG [48]:

$$Q_e = \frac{Q_{max} k_L C_e}{(1 + k_L C_e)} \quad \text{Langmuir} \quad (3)$$

$$Q_e = k_F C_e^{1/n} \quad \text{Freundlich} \quad (4)$$

$$Q_e = \left(\frac{RT}{B_t}\right) \ln(k_t C_e) \quad \text{Temkin} \quad (5)$$

where Q_{max} (mg/g) refers to the maximum adsorption capacity determined by Langmuir, k_L (L/mg) is the Langmuir isotherm constant, k_F ((mg/g)(mg/L)^{1/n}) is the Freundlich isotherm constant, and n (dimensionless and $n = 1$) is the constant governing heterogeneity and adsorption intensity. The universal gas constant is R (8.314 J/mol. Kelvin), the Temkin isotherm binding constant is k_t (L/g), the Temkin isotherm constant is B_t (J/mol), and the absolute reaction temperature is T (temperature in K). To further comprehend the adsorption process, the Langmuir separation factor (R_L) was also determined using Equation (6). The R_L expresses (dimensionless) the favorability of the Langmuir model-based adsorption process. $R_L = 0$ denotes the irreversible adsorption, whereas $R_L = 1$ promotes the linear adsorption. For there to be favorable adsorption, $0 < R_L < 1$.

$$R_L = \frac{1}{(1 + C_i K_L)} \quad (6)$$

For the best fit of the experimental data with the aforementioned models, in addition to a linear fitting, a nonlinear regression was also investigated. Additionally, this regression was taken into account to prevent mistakes from the nonlinear/linear transformation [49]. Based on the lowest Akaike Information Criterion (AIC) value calculated, using Equation (7), this criterion for nonlinear regression is the most precise and trustworthy statistical comparison measure to compare the best-fitting models with the experimental data [50]:

$$AIC = 2K + N \ln\left(\frac{SSE}{N}\right) + \frac{2K(K+1)}{(N-K-1)} \quad (7)$$

where N refers to the number of experimental points, K denotes the total number of model parameters, and SSE stands for the Sum of Squared Errors, which is calculated as:

$$SSE = \sum_i^N \left(Q_e^{experimental} - Q_e^{model} \right)^2 \quad (8)$$

3. Results and Discussion

3.1. Morphological Study of the Greener PG

Morphological characterizations illustrated in ref. [47] confirmed the successful synthesis of greener PG obtained via a near-green technique. Herein, the BET SSA of this greener PG was obtained to understand the importance of greener PG's SSA in the adsorption of contaminants. Figure 1 depicts the isotherms and Barret Joyner Halenda pore size distributions of greener PG. As per the given IUPAC classification, the N_2 adsorption-desorption isotherms curves for the greener PG sample demonstrated type IV with an H3 hysteresis loop revealing the same characteristics feature for mesopores [51,52]. The adsorption segment of the nitrogen isotherms at P/P_0 showed a fast increase, implying the formation of large mesopores and macropores [51,53], with pore width calculated as 3–5 nm. The rest of the parameters of the greener PG sample obtained from the N_2 adsorption-desorption isotherms are shown in Table S2. The BET SSA of the greener PG was calculated as circa $289.146 \text{ m}^2\text{g}^{-1}$, which is significantly higher than that of the previously reported commercial rGO-derived PG (circa $82.76 \text{ m}^2\text{g}^{-1}$) [3,54,55]. This proved that the sample showed a porous morphology with a bi-layer structure, which in turn resulted in a large number of active adsorption sites for the electrostatic reaction and finally boosted the adsorption mechanism.

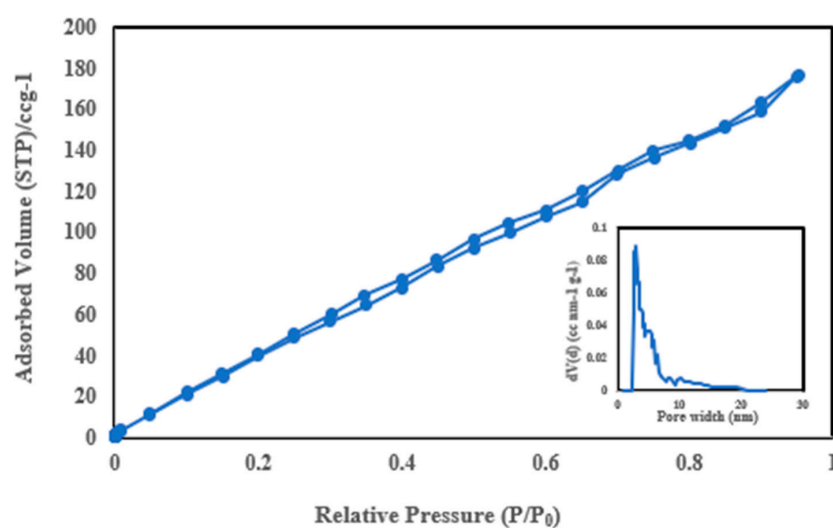


Figure 1. Measurement of the specific surface area. The pore size distribution of greener PG was calculated using the Barrett–Joyner–Halenda method as an inset at 77 K, with a pore size of 1–4 nm.

3.2. Adsorption Performance

3.2.1. Effect of Contact Time on the Contaminants' Removal

The effect of contact time on the adsorption of AT, CB, CPF, IBU, MeO, MeR, and RD onto greener PG for different time intervals, i.e., 5–120 min, are shown in Figure 2. A fast sorption rate (>90%) was seen during the first 40–50 min. Thus, for batch study, 120 min was the adequate period for the adsorption of these ECs onto greener PG. In total, 1 mL of greener PG dosage was used for all seven ECs to study the effect of contact time on the sorption performance of greener PG. Figure 2 shows concentration profiles at different contact time 't' (C_t) for ECs: AT, CB, CPF, and IBU. Fast sorption kinetics for the initial period of 60 min (indicating maximum adsorption) was observed for these four ECs, and then the adsorption rate declined with increasing time, prior to saturating after

60–80 min. Similarly, Figure 2, for dyes, MeO, MeR, and RD depict faster sorption kinetics for the initial period of 40 min and then the adsorption rate plummets with an increase in the contact time period. The results indicated an excellent adsorption performance of greener PG for these ECs, which was attributed to the availability of surface pores on the greener PG, reflected by its BET SSA in Figure 1. To further illustrate the sorption kinetics, two models (Equations (1) and (2)), i.e., pseudo first-order (Supplementary-S1) and pseudo second-order (Figure 3), were studied to understand the reaction kinetics of the seven ECs removal by the greener PG [48]. Of these models, the pseudo second-order rate model fitted the best for outlining the kinetic sorption of the seven tested ECs onto greener PG, as shown by the highest correlation coefficient values ($R^2 = 0.99$). Moreover, the Q_e (adsorption capacity at equilibrium) values calculated for all seven pollutants, for the pseudo second-order model, were in close proximity to the Q_e values obtained via the experiment. This indicates a linear relationship between t/Q_t and time (where Q_t is adsorption capacity at time 't'), reflecting the dependence of adsorption rate on adsorption capacity instead of adsorbate concentration. All the kinetic parameters for both models, along with their R^2 values, are listed in Table 1. Sorption kinetics can also be interpreted in terms of hydrophilicity and hydrophobicity of the adsorbents and contaminants, indicated by the n-octanol/water partition coefficient ($\log K_{ow}$ values) [56]. With the help of this indicator, it has previously been proven that IBU is hydrophobic [31], while CB [31] and MeR [57] both have a hydrophobic/phallic nature, which facilitates the adsorption kinetics with greener PG (having a super-hydrophobic nature). Similarly, the dyes, MeO and RD are also proven to have a hydrophobic nature [58,59], reflecting their rapid adsorption kinetics. These hydrophobic interactions between hydrophobes and water cause the hydrophobes (greener PG and ECs of hydrophobic nature) to attract each other and orient away from water [31,60], thus increasing the adsorption performance of greener PG for these hydrophobic contaminants. On the contrary, the hydrophilic nature of CPF and AT [31] reflects the slightly low adsorption onto greener PG.

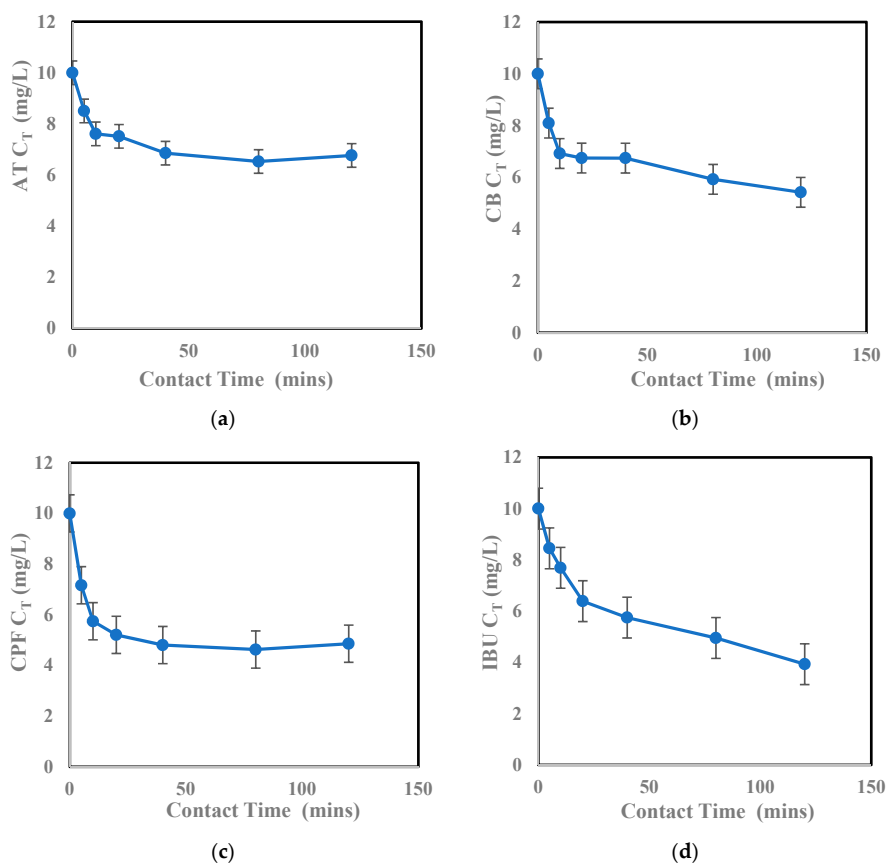


Figure 2. Cont.

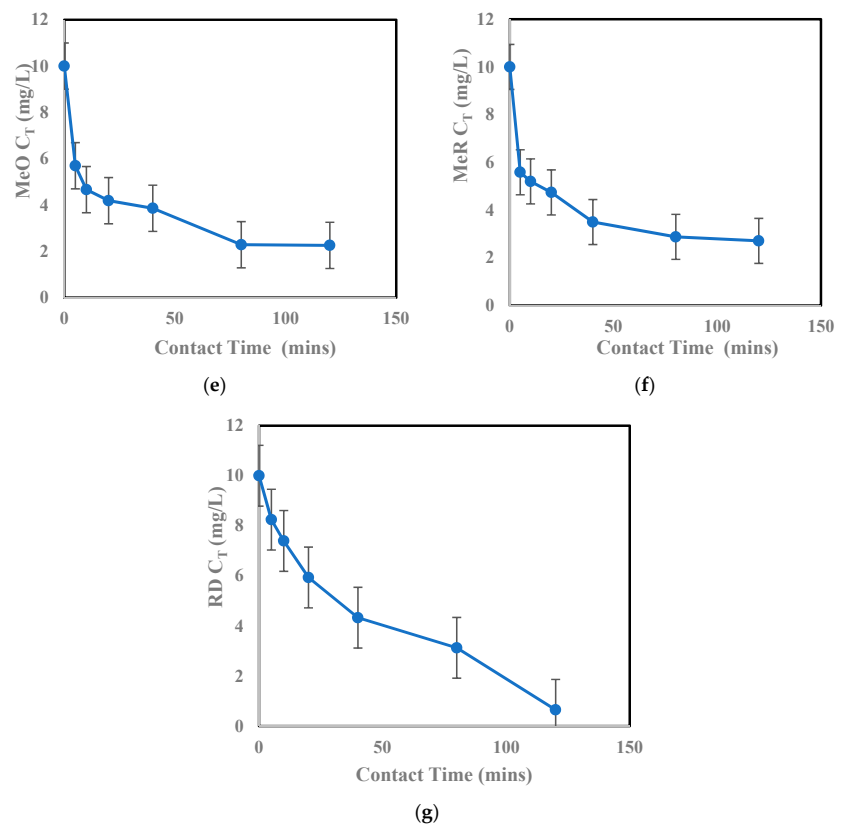


Figure 2. Effect of contact time on adsorption of the seven investigated emerging contaminants (10.0 mg/L) (a) AT; (b) CB; (c) CPF; (d) IBU; (e) MeO Dye; (f) MeR Dye; (g) RD Dye, onto 1.0 mL of greener PG solution (5 g/L).

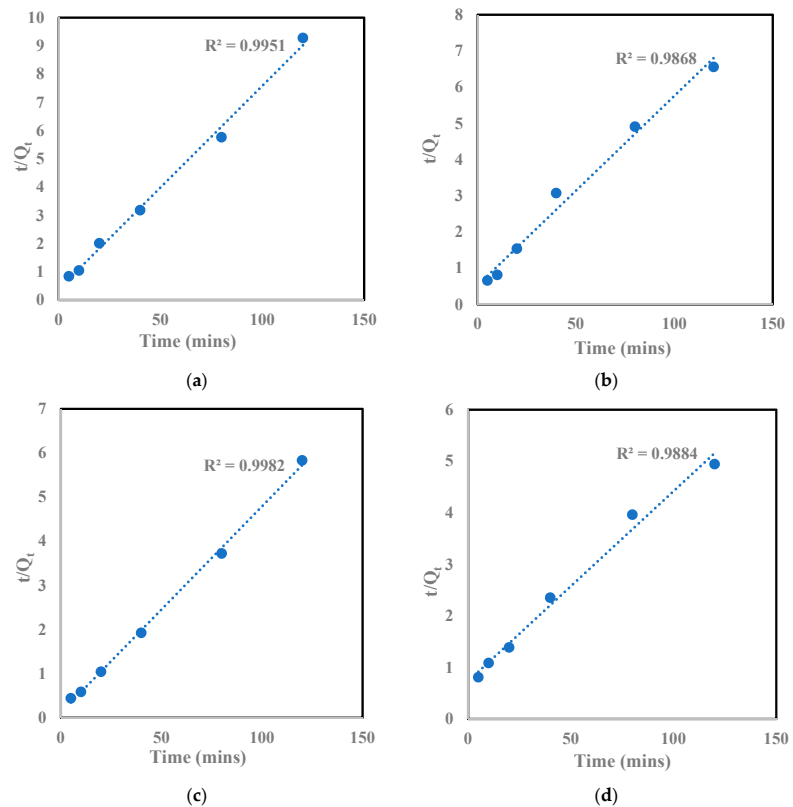


Figure 3. Cont.

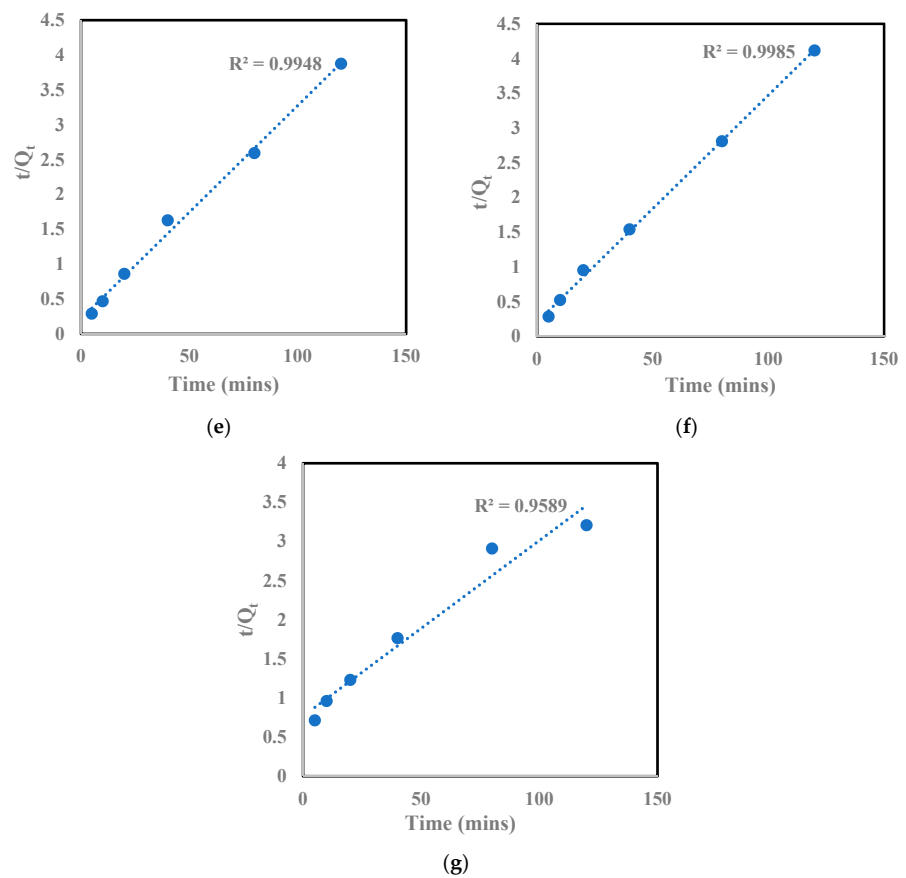


Figure 3. Pseudo second-order fitting for the seven tested emerging contaminants: (a) AT; (b) CB; (c) CPF; (d) IBU; (e) MeO Dye; (f) MeR Dye; (g) RD Dye.

Table 1. Kinetic parameters obtained for the two models, for emerging contaminants adsorption onto greener PG. R^2 is defined as the accuracy of the fitted model.

Contaminant Adsorbed onto Greener PG	Pseudo First-Order					Pseudo Second-Order				
	R^2	Slope	Intercept	Q_e (mg/g)	K_1 (1/mins)	R^2	Slope	Intercept	Q_e (mg/g)	K_2 (g/mg mins)
AT	0.54	0.028	1.89	6.621	−0.0002	<u>0.99</u>	0.07	0.38	13.38	0.0020
CB	0.90	−0.01	2.54	12.72	−0.001	<u>0.98</u>	0.05	0.523	19.09	696.53
CPF	0.56	−0.02	1.93	6.94	−0.0002	<u>0.99</u>	0.04	0.11	21.38	3962.14
IBU	0.94	−0.02	3.10	22.2	−0.0001	<u>0.98</u>	0.03	0.73	27.11	1005.0
MeO	0.94	−0.04	3.06	21.45	−0.0003	<u>0.99</u>	0.03	0.21	32.70	0.0002
MeR	0.97	−0.03	2.89	18.02	−0.0003	<u>0.99</u>	0.03	0.20	30.59	4574.6
RD	0.82	−0.03	3.89	49.27	−0.0003	<u>0.95</u>	0.002	0.76	44.54	2582.82

3.2.2. Effect of Various Adsorbent Dosages on Contaminant Removal

To understand the removal potency of this greener PG, a batch adsorption test was conducted on these seven ECs for six different dosages of greener PG (0.5 mL, 1 mL, 1.5 mL, 2 mL, 2.5 mL, and 3 mL of adsorbent injected from a 5-g/L suspension). The results are shown in Figure 4. The experiment was run for 24 h to ensure that each of the contaminants reached its equilibrium. For all the contaminants, the experimental conditions were the same and are listed below in Figure 4. The figure shows that with the increase in adsorbent dosage, the removal efficiency for these seven tested ECs increased. Greener PG showed a greater removal efficiency (between 85–95%) for dyes (MeO, MeR, and RD) than for ECs (AT,

CPF, CB, and IBU). Among the dyes, MeO and RD showed the highest removal efficiency (>90%) by greener PG, resulting from hydrophobe–hydrophobe attraction between greener PG and these two dyes. The greener PG showed an effective removal potency for the four ECs, i.e., AT, CPF, CB, and IBU, with a removal efficiency between 70 and 90%, and IBU showing the highest removal efficiency (94.4%), which is attributed to its hydrophobic nature. Table S1 summarizes the full data of the removal efficiency of the adsorbent for these seven ECs with varying greener PG dosages. These seven emerging contaminants were also tested against the commercially obtained PG and are illustrated in Figure 5. Commercial PG showed less adsorption for each of these ECs as compared to greener PG. This could be attributed to the low specific surface area of the commercial PG mentioned in Section 3.1. Greener PG exhibited large meso- and macro-pores, which increased the overall surface area of this greener adsorbent and further acted as an adsorption site for the seven ECs.

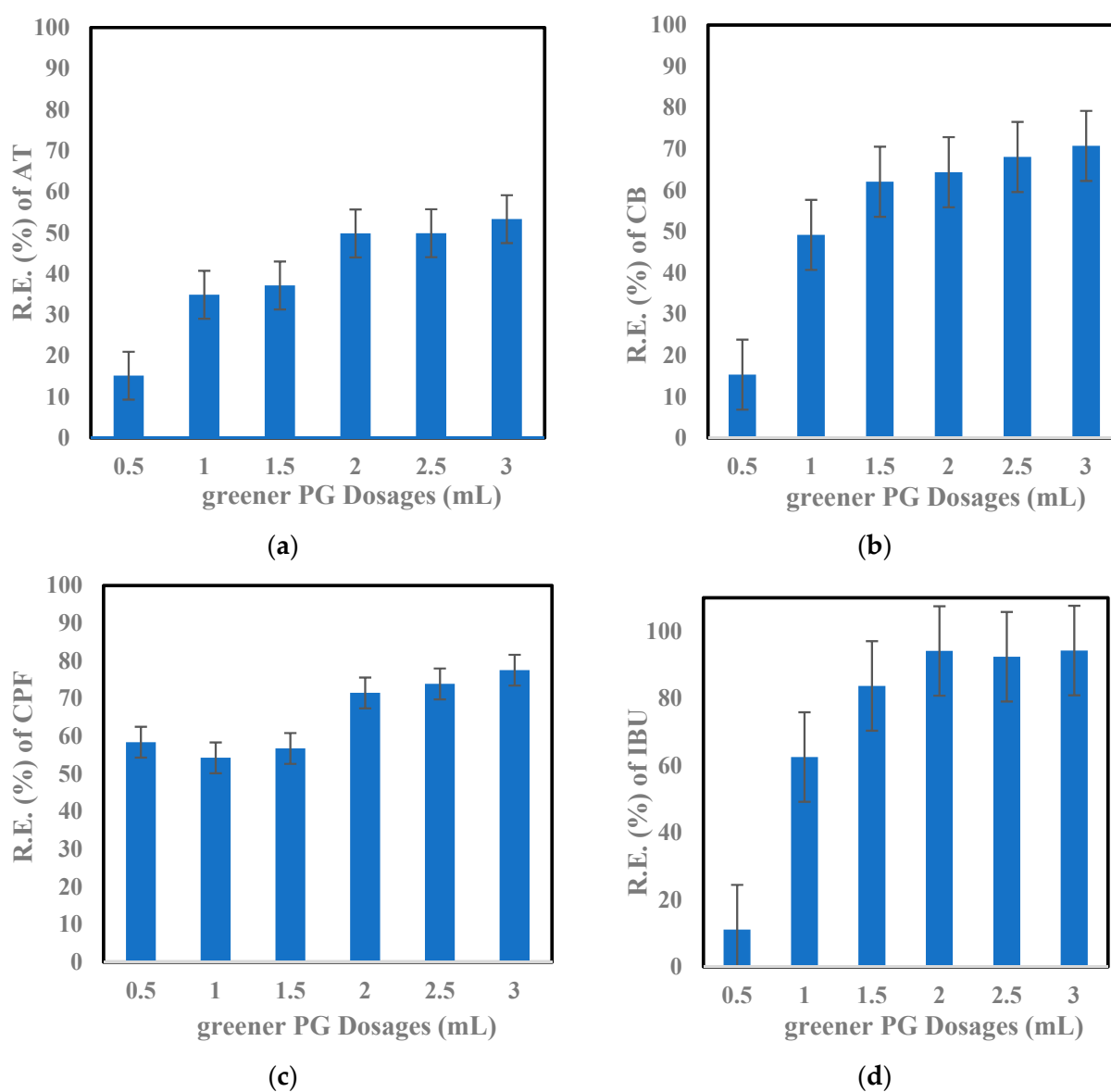


Figure 4. Cont.

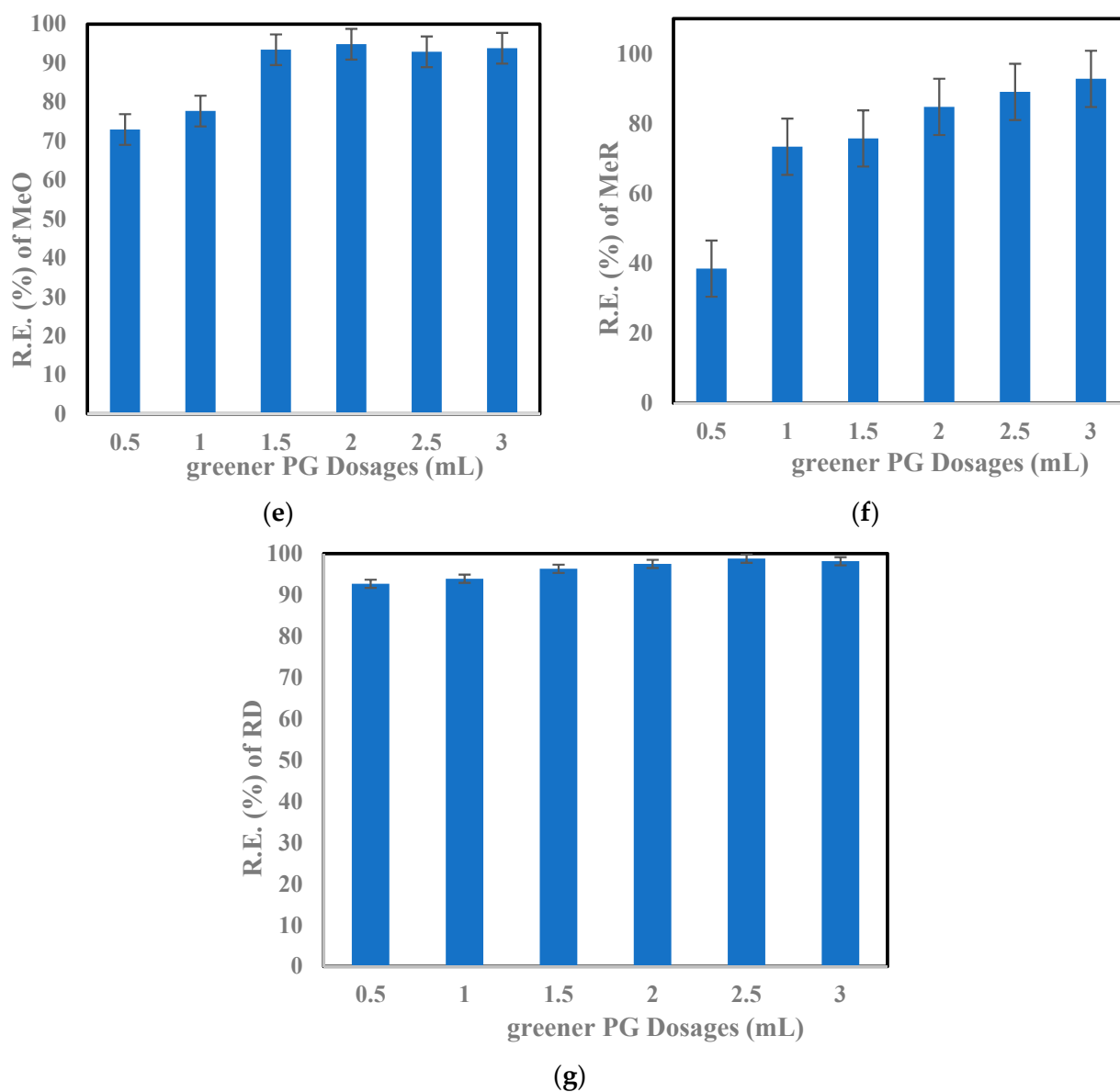


Figure 4. Equilibrium study for the seven tested emerging contaminants depicting their removal efficiency with varying greener PG Dosages: (a) AT; (b) CB; (c) CPF; (d) IBU; (e) MeO; (f) MeR; (g) RD.

After reaching the equilibrium, the concentration (C_{eq}) of each of these ECs was obtained at varying greener PG dosages. The concentration profiles for each of the seven tested ECs with various adsorbent doses are shown in Figure 6. All these seven contaminants displayed similar profiles, i.e., the concentration (C_{eq}) of each of these ECs decreased with the increasing doses of greener PG, indicating maximum EC adsorption at the highest greener PG dosage. This increase in adsorption with an increase in adsorbent dosages was aided by the adsorption capacity (Q_e) curves for each EC shown in Figure 7. Contaminants IBU, MeO, and RD exhibit similar adsorption profiles, indicating their highest removal with maximum adsorption capacities: 37.86 mgg^{-1} (Figure 7d), 38 mgg^{-1} (Figure 7e), and 39.5 mgg^{-1} (Figure 7g), respectively. A very minimal variation in adsorption capacity was observed after 2 mL of greener PG dosage, contributing to nearly identical removal efficiencies of the contaminants for other two higher greener PG dosages. This proves that this greener PG obtained from near-green synthesis showed a considerable potential for water treatment application.

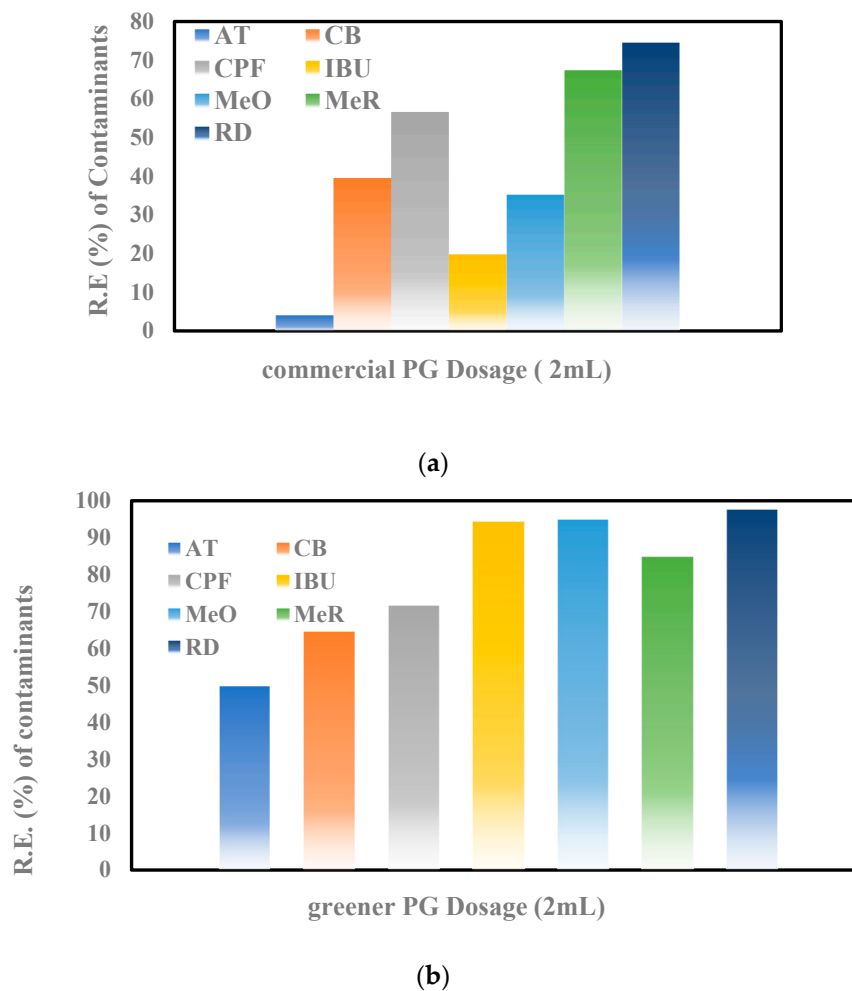


Figure 5. Equilibrium study for the seven tested emerging contaminants depicting their removal efficiency with varying (a) commercial PG Dosages and (b) greener PG Dosages.

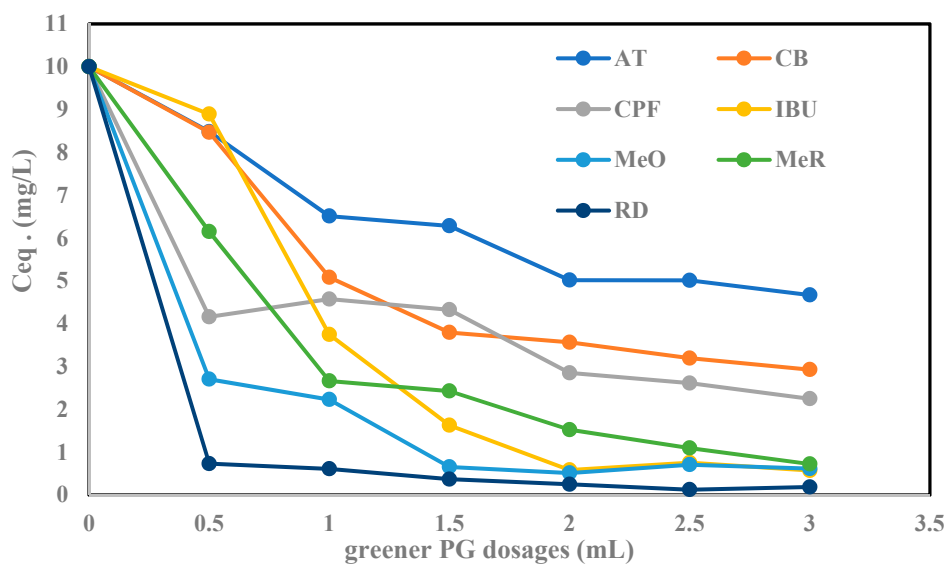


Figure 6. Equilibrium concentration (mg/L) for the seven investigated contaminants vs. greener PG dosages (mL).

To study the adsorption behavior of greener PG, adsorption isotherms for each of these seven ECs were investigated [61]. In this study, we examined three models—Langmuir (Equation (3)), Freundlich (Equation (4)), and Temkin (Equation (5)), in both their linear and nonlinear forms [48–50]. In the case of linear modeling, the best-fitted adsorption model was expressed with the help of linear correlation coefficient R^2 and other intrinsic parameters, which are listed in Table S3. The Temkin model for all seven contaminants was eliminated, as the intrinsic parameter, B_t , showed negative values [54,62,63]. For all the seven tested contaminants, the R^2 values for these three models are highlighted in Table S3.

According to the values obtained for R^2 (>0.9), Freundlich and Langmuir showed the best fit for CPF, MeO, and RD contaminants, and the Freundlich model fitted the best for the contaminants AT, CB, IBU, and MeR, confirming multilayer adsorption of these contaminants onto greener PG. However, based on the other intrinsic parameters shown in Table S3, RD followed the Langmuir model as it showed a negative slope in the case of the Freundlich isotherm model, confirming the monolayer adsorption of the dye RD onto the greener PG [61].

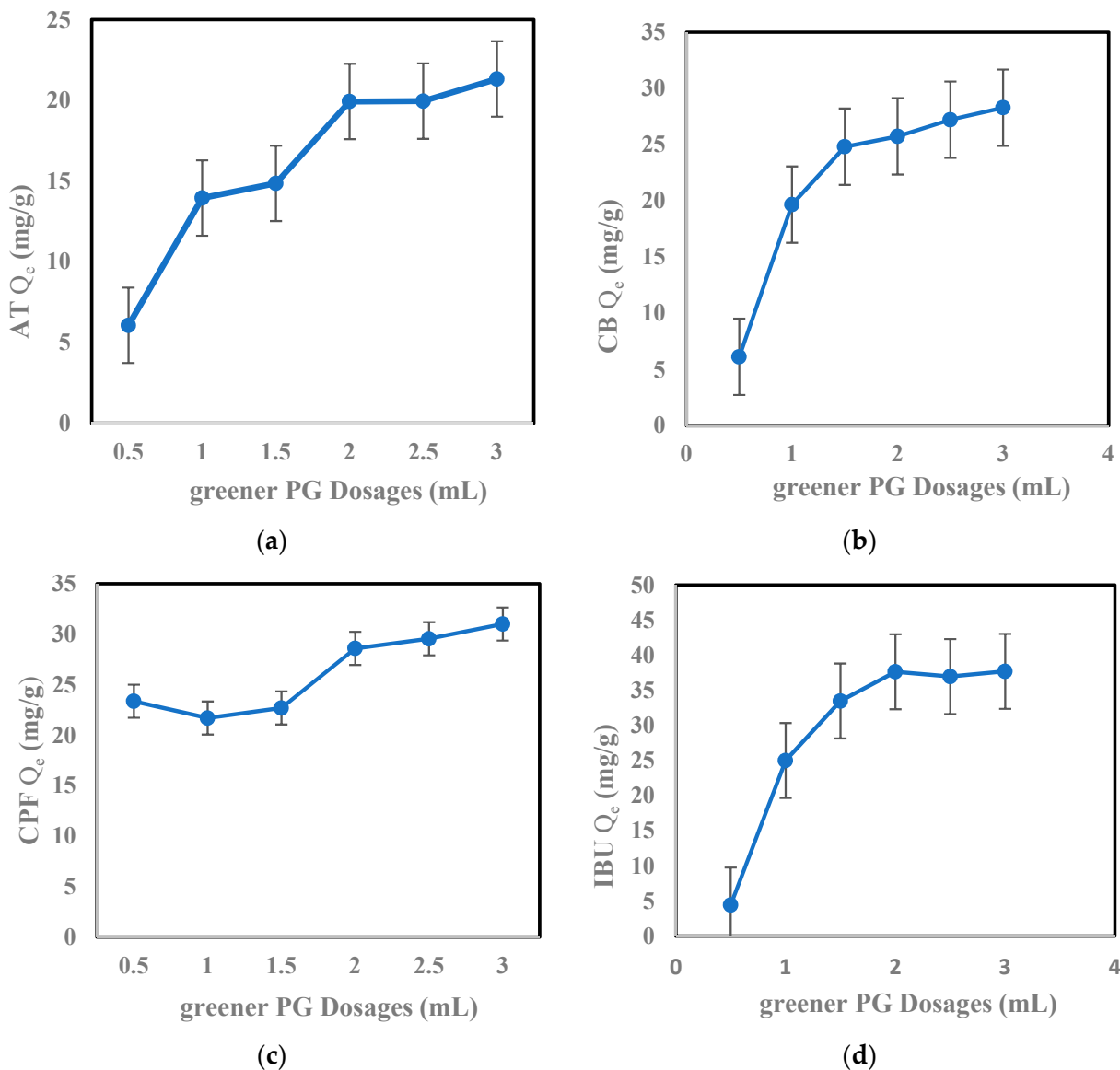


Figure 7. Cont.

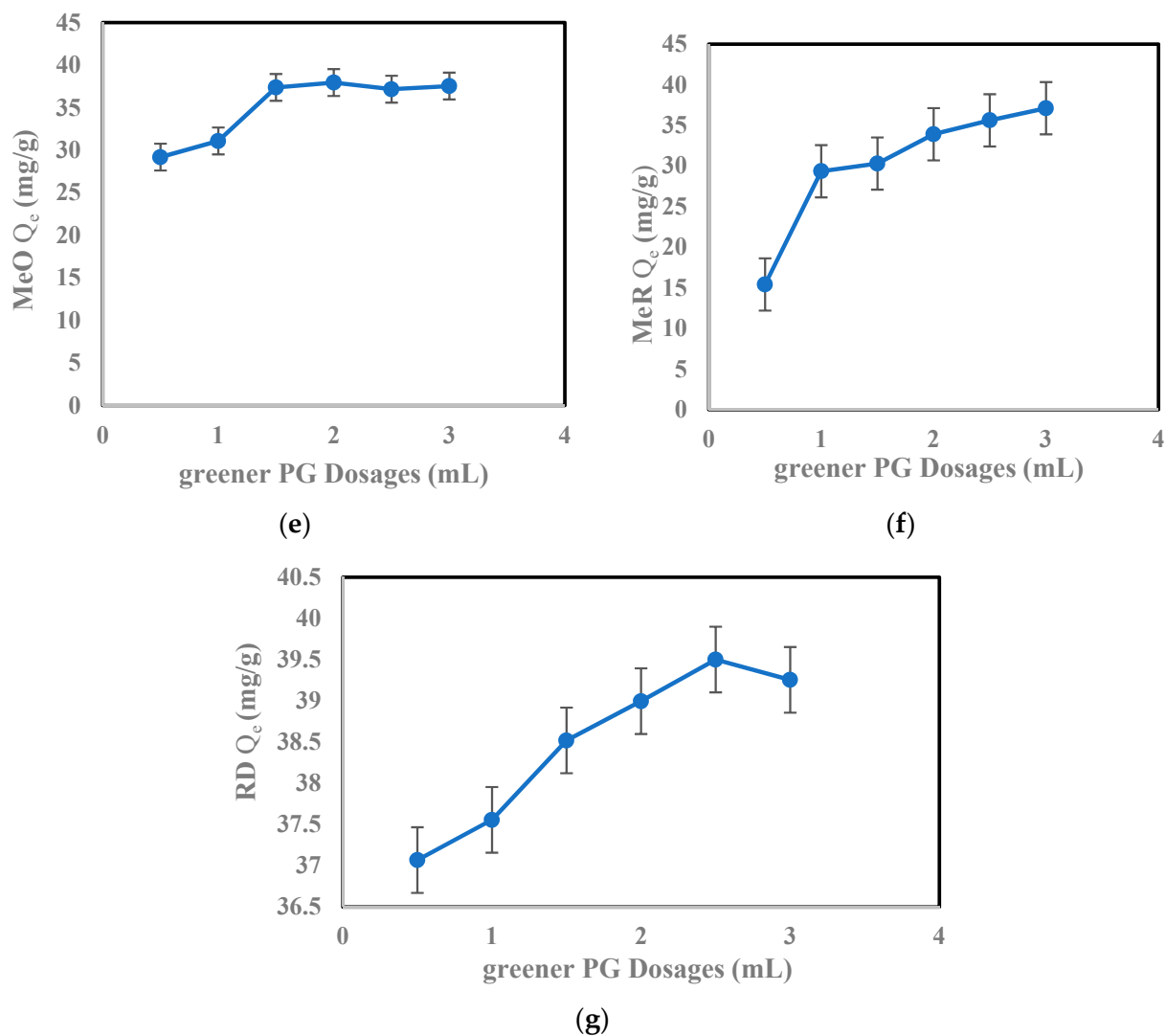


Figure 7. Adsorption curve for seven tested contaminants at different greener PG dosages (mL): (a) AT; (b) CB; (c) CPF; (d) IBU; (e) MeO; (f) MeR; (g) RD.

The nonlinear modeling was also studied for these three models [49,50]. Freundlich's model showed the best fit for all the contaminants, except RD. For the six contaminants AT, CPF, CB, IBU, MeO, and MeR, a positive value of slope and the lowest AIC values (obtained from Equations (7) and (8)) were obtained for the Freundlich model, indicating the possibility of the involvement of physisorption in the adsorption process and heterogeneity in the greener PG surface. Separation factor values, R_L , were also obtained for these six contaminants and showed either more than 1 or less than zero values, further indicating the Freundlich model being the best suited for these six ECs. RD showed the lowest AIC value for the Langmuir model, indicating the monomolecular adsorption on greener PG surface without any dye stacking. This was further confirmed with separation factor ($R_L = 0.94$), obtained between 0 and 1, and contributing to the favorable adsorption process. This showed the possibility of a binary [63] sorption mechanism. The AIC values (highlighted as being the best-suited model) and other nonlinear intrinsic parameters were calculated for all seven contaminants (Table 2).

Table 2. Nonlinear adsorption isotherm parameters for all seven emerging contaminants removal by greener PG. Lowest AIC values are highlighted for the best-suited model.

CONTAMINANT	Freundlich Isotherm Model	Langmuir Isotherm Model	Temkin Isotherm Model
ATENOLOL (AT)	K_f ((mg/g) {mg/L} ^{1/m}) = 1.82 $m = 1/n = 1$ $R^2 = 0.93$ AIC = 40.89	Q_{max} (mg/g) = 3.79 K_i (l/mg) = -0.24 $R_L = -0.697878596$ $R^2 = 0.77$ AIC = 26.90	K_t (L/mg) = 0.90 B_t (J/mol) = -25.32 $R^2 = 0.92$ AIC = 54.22
CARBAMAZEPINE (CB)	K_f ((mg/g) {mg/L} ^{1/m}) = 2.31 $m = 1/n = 1$ $R^2 = 0.92$ AIC = 44.94	Q_{max} (mg/g) = 5.15 K_i (l/mg) = -9.77 $R_L = -0.010334966$ $R^2 = 0.73$ AIC = 42.8	K_t (L/mg) = 0.083 B_t (J/mol) = -20.99 $R^2 = 0.98$ AIC = 63.99
IBUPROFEN (IBU)	K_f ((mg/g) {mg/L} ^{1/m}) = 2.764 $m = 1/n = 1$ $R^2 = 0.764$ AIC = 48.51	Q_{max} (mg/g) = 7.61 K_i (l/mg) = -0.0104 $R_L = 1.116444$ $R^2 = 0.390$ AIC = 49.39	K_t (L/mg) = 0.04 B_t (J/mol) = -11.55 $R^2 = 0.89$ AIC = 83.40
CIPROFLOXIN (CPF)	K_f ((mg/g) {mg/L} ^{1/m}) = 6.79 $m = 1/n = 1$ $R^2 = 0.98$ AIC = 35.91	Q_{max} (mg/g) = 17.15 K_i (l/mg) = -0.003 $R_L = 1.037482$ $R^2 = 0.95$ AIC = 43.37	K_t (L/mg) = 0.041 B_t (J/mol) = -13.26 $R^2 = 0.99$ AIC = 77.76
METHYL RED (MeR)	K_f ((mg/g) {mg/L} ^{1/m}) = 4227.29 $m = 1/n = 1$ $R^2 = 0.82$ AIC = 121.44	Q_{max} (mg/g) = 19.799 K_i (l/mg) = -0.0011 $R_L = 1.98879407$ $R^2 = 0.46$ AIC = 49.26	K_t (L/mg) = 0.024 B_t (J/mol) = -9.911 $R^2 = 0.89$ AIC = 87.26
METHYL ORANGE (MeO)	K_f ((mg/g) {mg/L} ^{1/m}) = 17.44 $m = 1/n = 1$ $R^2 = 0.98$ AIC = 45.73	Q_{max} (mg/g) = 28.52 K_i (l/mg) = -0.00018 $R_L = 1.00178603$ $R^2 = 0.92$ AIC = 50.74	K_t (L/mg) = 0.001 B_t (J/mol) = -5.31 $R^2 = 0.988$ AIC = 104.06
RHODAMINE-B (RD)	K_f ((mg/g) {mg/L} ^{1/m}) = 75.77 $m = 1/n = 1$ $R^2 = 0.98$ AIC = 58.0	Q_{max} (mg/g) = 155.54 K_i (l/mg) = 24197.99 $R_L = 1.03314 \times 10^{-6}$ $R^2 = 0.94$ AIC = 23.72	K_t (L/mg) = $2.9 \times e^{-10}$ B_t (J/mol) = -7.122 $R^2 = 0.98$ AIC = 114.59

Therefore, both linear and nonlinear modeling implied that the adsorption process was governed by nonlinearity in the adsorption of seven ECs onto greener PG. Unlike the PG obtained via the Hummers method, which has shown the heterogenous behavior (following Sips and Toth models) in the adsorption process [31], the removal process by the greener PG followed the Freundlich adsorption model for most of the contaminants with potential involvement of both physio/chemisorption.

Table 3 summarizes the various carbon-based adsorbents in ascending order of their BET-SSA, for water treatment applications. The greener PG, synthesized in this research, had the third highest BET-SSA when compared with other adsorbents, and showed higher adsorption capacity for these seven EC in comparison to especially MWCNT and commercial PG. The greener PG also showed a comparable result with PG derived from the Hummers method, with the added advantage of being a risk-free adsorbent to the environment. RAG, of the synthesis process, is also depicted in the table, demonstrating the environmentally friendly nature of the synthesis process. Of all the synthesis processes describing their RAG to be Green (G), greener PG is the only adsorbent with high BET-SSA. Thus, this adsorbent can be an easy alternative to many adsorbents belonging to the carbon family, with comparable removal efficacy towards emerging pollutants removal.

Table 3. Comparison table of the adsorbents depicted in ascending order of their BET SSA, for water treatment application.

ADSORBENT MATERIAL	BET SSA (m ² /g)	Contaminants Tested for Adsorption/Absorbate	ADSORPTION CAPACITY (mg/g)	References	RAG of Synthesis Process R—Red A—Amber G—Green
Graphite	4.5	Carbamazepine—CB Methyl Orange—MeO	CB—3.65 ± 0.05 MeO—13.6	[64–66]	G
Commercial Graphene	15	Carbamazepine—CB Methyl Orange—MeO Ciprofloxacin—CPF Atenolol—AT Ibuprofen—IBU	CPF—323 AT—<6 IBU—6.0 CB—22.8 ± 0.5 MeO—89.3	[66–69]	A
Graphene Oxide (GO)	38	Carbamazepine—CB Methyl Orange—MeO Ciprofloxacin—CPF Atenolol—AT Ibuprofen—IBU Methyl Red—MeR Diclofenac—DCF Rhodamine b—RD Gemfibrozil—GEM	CPF—417.79 AT—7.598 GEM—2.981 IBU—10.01 DCF—3.65 CB—8.89 MeR—63.69 MeO—16.83 RD—0.54	[31,67,70,71]	R
Chemically reduced Graphene Oxide (rGO)	53	Ciprofloxacin—CPF Carbamazepine—CB Methyl Orange—MeO Diclofenac sodium—DCFS Malachite Green—MG	CPF—18.2 DCFS—59.67 CBZ—55.13 MG—279.85 MeO—244	[72–77]	R
Commercial Porous Graphene (PG)	82.76	Carbamazepine—CB Methyl Orange—MeO Methyl Red—MeR Ciprofloxacin—CPF Atenolol—AT Ibuprofen—IBU Rhodamine b—RD	CPF—11.34 CB—7.92 AT—0.84 IBU—3.976 MeO—7.06 MeR—13.48 RD—4.872	This paper	A,R
Multi walled Carbon nanotube—MWCNT	160	Carbamazepine—CB Methyl Orange—MeO Ibuprofen—IBU Ciprofloxacin—CPF	CPF—1.745 CBU—108 MeO—27.6 IBU—186.5	[68,73,78,79]	A,R
GREENER PG	289.14	Ciprofloxacin—CPF Methyl Orange—MeO Methyl Red—MeR Rhodamine b—RD Atenolol—AT Ibuprofen—IBU Carbamazepine—CB	CPF—28.596 CB—25.74 AT—19.29 IBU—37.65 MeO—37.16 MeR—84.75 RD—38.52	This paper	G
Porous Graphene	679	Ciprofloxacin—CPF Rhodamine b—RD Atenolol—AT Ibuprofen—IBU Carbamazepine—CB Gemfibrozil—GEM Diclofenac—DCF	CPF—370.11 AT—2.738 GEM—4.604 IBU—47.85 DCF—41.23 CB—88.96 RD—16.6 × 10 ⁴	[31]	R
Activated Carbon	1156	Ciprofloxacin—CPF Diclofenac—DCF Carbamazepine—CB Ibuprofen—IBU Methyl Red—MeR	CPF—1.860 DCF—56.2 CB—3.2 MeR—10.0 IBU—12.6	[68,80–82]	R

Thus, this research investigated and summarized an efficacy of the greener PG as an excellent adsorbent candidate for the removal of emerging contaminants in water treatment applications.

4. Conclusions and Outlook

This study aimed to explore the removal of seven emerging contaminants, i.e., atenolol, ciprofloxacin, ibuprofen, carbamazepine, methyl orange, methyl red, and rhodamine-B, by the greener PG, synthesized via a near-green synthesis method. The BET analysis showed high specific surface of $289.146 \text{ m}^2\text{g}^{-1}$ and confirmed porous morphology with a bi-layer structure of the greener PG. The potency of this greener PG in water treatment application was explored by obtaining adsorption profiles for different batch conditions: (i) contact time, and (ii) adsorbent dosage. Both linear and nonlinear modeling methods were applied to avoid any error. The study revealed that:

- (i) Fast sorption kinetics are followed by a pseudo second-order model;
- (ii) With the increase in greener PG dosage, adsorption of the investigated contaminants increases;
- (iii) Langmuir model fitted best for rhodamine-b dye, confirming the monomolecular adsorption on the greener PG surface and no stacking of the adsorbed dye;
- (iv) The remaining six contaminants followed the Freundlich model, involving a possibility of physisorption;
- (v) Overall, removal efficiency of the greener PG showed better performance when compared with commercial rGO-obtained PG, for all the seven contaminants.

Despite these encouraging findings, there is a need to explore the long-term effects of the commercially available and greener PG in the aquatic environment.

Supplementary Materials: The following supporting information can be downloaded at: <https://www.mdpi.com/article/10.3390/c9040097/s1>, S1. Kinetic pseudo first-order modeling graphs. Figure S1: Pseudo first-order model for: (a) Contaminant AT; (b) Contaminant CB; (c) Contaminant CPF; (d) IBU; (e) Contaminant MeO; (f) Contaminant MeR; (g) Contaminant RD. Table S1: Summary of Equilibrium study of greener PG on seven emerging contaminants. Table S2: Parameters of the greener PG sample obtained from the N₂ adsorption–desorption isotherms. Table S3: Linear adsorption isotherm parameters for all seven contaminants; removal by greener PG.

Author Contributions: Conceptualization, B.J. and A.M.E.K.; Methodology, B.J.; Formal analysis, B.J.; Investigation, B.J.; Data curation, B.J.; Writing—original draft, B.J.; Writing—review & editing, B.J., A.M.E.K., S.Z. and F.A.M.; Visualization, B.J.; Supervision, S.Z. and F.A.M.; Project administration, S.Z. and F.A.M.; Funding acquisition, S.Z. and F.A.M. All authors have read and agreed to the published version of the manuscript.

Funding: This research was supported by the FAME (Fate and Management of Emerging Contaminants) Project, jointly funded by UK Natural Environment Research Council (NE/R003548/1) and the Department of Science and Technology, Government of India (DST/TM/INDO-UK/2K17/66(C)).

Data Availability Statement: The data presented in this study are available on request from the corresponding author.

Conflicts of Interest: The authors declare no competing financial interests.

References

1. Filho, W.L.; Ellams, D.; Han, S.; Tyler, D.; Boiten, V.J.; Paco, A.; Moora, H.; Balogun, A.L. A review of the socio-economic advantages of textile recycling. *J. Clean. Prod.* **2019**, *218*, 10–20. [[CrossRef](#)]
2. Cooter, R.; Pickstone, J. (Eds.) *Companion to Medicine in the Twentieth Century*, 1st ed.; Routledge: Oxfordshire, UK, 2002. [[CrossRef](#)]
3. Tabish, T.A.; Memon, F.A.; Gomez, D.E.; Horsell, D.W.; Zhang, S. A facile synthesis of porous graphene for efficient water and wastewater treatment. *Sci. Rep.* **2018**, *8*, 1817. [[CrossRef](#)] [[PubMed](#)]
4. UNICEF Division of Global Communication and Advocacy. *Triple Threat How Disease, Climate Risks, and Unsafe Water, Sanitation and Hygiene Create a Deadly Combination for Children*; United Nations Children’s Fund (UNICEF): New York, NY, USA, 2023; Available online: www.unicef.org (accessed on 31 March 2023).
5. Iwuozor, K.O.; Ighalo, J.O.; Emenike, E.C.; Ogunfowora, L.A.; Igwegbe, C.A. Adsorption of methyl orange: A review on adsorbent performance. *Curr. Res. Green Sustain. Chem.* **2021**, *4*, 100179. [[CrossRef](#)]
6. Shetty, D.; Jahovic, I.; Raya, J.; Ravaux, F.; Jouiad, M.; Olsen, J.C.; Trabolsi, A. An ultra-absorbent alkyne-rich porous covalent polycalix[4]arene for water purification. *J. Mater. Chem. A Mater.* **2017**, *5*, 62–66. [[CrossRef](#)]

7. Dutta, S.K.; Amin, M.K.; Ahmed, J.; Elias, M.; Mahiuddin, M. Removal of toxic methyl orange by a cost-free and eco-friendly adsorbent: Mechanism, phytotoxicity, thermodynamics, and kinetics. *S. Afr. J. Chem. Eng.* **2022**, *40*, 195–208. [[CrossRef](#)]
8. Muthuraman, G.; Teng, T.T. Extraction of methyl red from industrial wastewater using xylene as an extractant. *Prog. Nat. Sci.* **2009**, *19*, 1215–1220. [[CrossRef](#)]
9. Singh, S.; Parveen, N.; Gupta, H. Adsorptive decontamination of rhodamine-B from water using banana peel powder: A biosorbent. *Environ. Technol. Innov.* **2018**, *12*, 189–195. [[CrossRef](#)]
10. Zuccato, E.; Calamari, D.; Natangelo, M.; Fanelli, R. Presence of therapeutic drugs in the environment. *Lancet* **2000**, *355*, 1789–1790. [[CrossRef](#)]
11. Daughton, C.G. Non-regulated water contaminants: Emerging research. *Environ. Impact Assess. Rev.* **2004**, *24*, 711–732. [[CrossRef](#)]
12. Fent, K.; Weston, A.A.; Caminada, D. Ecotoxicology of human pharmaceuticals. *Aquat. Toxicol.* **2006**, *76*, 122–159. [[CrossRef](#)]
13. Oki, T.; Kanae, S. Global hydrological cycles and world water resources. *Science* **2006**, *313*, 1068–1072. [[CrossRef](#)] [[PubMed](#)]
14. Kümmerer, K. The presence of pharmaceuticals in the environment due to human use—Present knowledge and future challenges. *J. Environ. Manag.* **2009**, *90*, 2354–2366. [[CrossRef](#)] [[PubMed](#)]
15. Li, W.C. Occurrence, sources, and fate of pharmaceuticals in aquatic environment and soil. *Environ. Pollut.* **2014**, *187*, 193–201. [[CrossRef](#)]
16. Lapworth, D.J.; Baran, N.; Stuart, M.E.; Ward, R.S. Emerging organic contaminants in groundwater: A review of sources, fate and occurrence. *Environ. Pollut.* **2012**, *163*, 287–303. [[CrossRef](#)] [[PubMed](#)]
17. Verlicchi, P.; Al Aukidy, M.; Zambello, E. Occurrence of pharmaceutical compounds in urban wastewater: Removal, mass load and environmental risk after a secondary treatment—A review. *Sci. Total Environ.* **2012**, *429*, 123–155. [[CrossRef](#)]
18. Rivera-Utrilla, J.; Sánchez-Polo, M.; Ferro-García, M.Á.; Prados-Joya, G.; Ocampo-Pérez, R. Pharmaceuticals as emerging contaminants and their removal from water. A review. *Chemosphere* **2013**, *93*, 1268–1287. [[CrossRef](#)] [[PubMed](#)]
19. Wilkinson, J.; Hooda, P.S.; Barker, J.; Barton, S.; Swinden, J. Occurrence, fate and transformation of emerging contaminants in water: An overarching review of the field. *Environ. Pollut.* **2017**, *231*, 954–970. [[CrossRef](#)]
20. Carpenter, C.M.G.; Helbling, D.E. Widespread Micropollutant Monitoring in the Hudson River Estuary Reveals Spatiotemporal Micropollutant Clusters and Their Sources. *Environ. Sci. Technol.* **2018**, *52*, 6187–6196. [[CrossRef](#)]
21. Bottoni, P.; Caroli, S. Presence of residues and metabolites of pharmaceuticals in environmental compartments, food commodities and workplaces: A review spanning the three-year period 2014–2016. *Microchem. J.* **2018**, *136*, 2–24. [[CrossRef](#)]
22. Schafhauser, B.H.; Kristofco, L.A.; de Oliveira, C.M.R.; Brooks, B.W. Global review and analysis of erythromycin in the environment: Occurrence, bioaccumulation and antibiotic resistance hazards. *Environ. Pollut.* **2018**, *238*, 440–451. [[CrossRef](#)]
23. Balakrishna, K.; Rath, A.; Praveenkumarreddy, Y.; Guruge, K.S.; Subedi, B. A review of the occurrence of pharmaceuticals and personal care products in Indian water bodies. *Ecotoxicol. Environ. Saf.* **2017**, *137*, 113–120. [[CrossRef](#)] [[PubMed](#)]
24. Miller, T.H.; Bury, N.R.; Owen, S.F.; MacRae, J.I.; Barron, L.P. A review of the pharmaceutical exposome in aquatic fauna. *Environ. Pollut.* **2018**, *239*, 129–146. [[CrossRef](#)] [[PubMed](#)]
25. Kolpin, D.W.; Furlong, E.T.; Meyer, M.T.; Thurman, E.M.; Zaugg, S.D.; Barber, L.B.; Buxton, H.T. Pharmaceuticals, hormones, and other organic wastewater contaminants in U.S. streams, 1999–2000: A national reconnaissance. *Environ. Sci. Technol.* **2002**, *36*, 1202–1211. [[CrossRef](#)] [[PubMed](#)]
26. Zwiener, C. Occurrence and analysis of pharmaceuticals and their transformation products in drinking water treatment. *Anal. Bioanal. Chem.* **2007**, *387*, 1159–1162. [[CrossRef](#)]
27. Nikolaou, A.; Meric, S.; Fatta, D. Occurrence patterns of pharmaceuticals in water and wastewater environments. *Anal. Bioanal. Chem.* **2007**, *387*, 1225–1234. [[CrossRef](#)]
28. Daughton, C.G. Cradle-to-cradle stewardship of drugs for minimizing their environmental disposition while promoting human health. I. Rational for and avenues toward a green pharmacy. *Environ. Health Perspect.* **2003**, *111*, 757–774. [[CrossRef](#)]
29. Simazaki, D.; Kubota, R.; Suzuki, T.; Akiba, M.; Nishimura, T.; Kunikane, S. Occurrence of selected pharmaceuticals at drinking water purification plants in Japan and implications for human health. *Water Res.* **2015**, *76*, 187–200. [[CrossRef](#)]
30. Fekadu, S.; Alemayehu, E.; Dewil, R.; Van der Bruggen, B. Pharmaceuticals in freshwater aquatic environments: A comparison of the African and European challenge. *Sci. Total Environ.* **2019**, *654*, 324–337. [[CrossRef](#)]
31. Khalil, A.M.E.; Memon, F.A.; Tabish, T.A.; Salmon, D.; Zhang, S.; Butler, D. Nanostructured porous graphene for efficient removal of emerging contaminants (pharmaceuticals) from water. *Chem. Eng. J.* **2020**, *398*, 125440. [[CrossRef](#)]
32. Del Rosario Brunetto, M.; Clavijo, S.; Delgado, Y.; Orozco, W.; Gallignani, M.; Ayala, C.; Cerdà, V. Development of a MSFIA sample treatment system as front end of GC-MS for atenolol and propranolol determination in human plasma. *Talanta* **2015**, *132*, 15–22. [[CrossRef](#)]
33. Velasco, M.; Romero, B.; Betancourt, M.; Suarez, N.; Contreras, F. Uso de los Antagonistas Beta-Adrenérgicos en la Hipertensión Arterial. *Arch. Venez. Farmacol. Ter.* **2002**, *21*, 139–147. Available online: http://ve.scielo.org/scielo.php?script=sci_arttext&pid=S0798-02642002000200002&lng=es&nrm=iso&tlng=es (accessed on 9 August 2023).
34. Meador, K.J.; Seliger, J.; Boyd, A.; Razavi, B.; Falco-Walter, J.; Le, S.; Loring, D.W. Comparative neuropsychological effects of carbamazepine and eslicarbazepine acetate. *Epilepsy Behav.* **2019**, *94*, 151–157. [[CrossRef](#)] [[PubMed](#)]
35. Pomati, F.; Castiglioni, S.; Zuccato, E.; Fanelli, R.; Vigetti, D.; Rossetti, C.; Calamari, D. Effects of a complex mixture of therapeutic drugs at environmental levels on human embryonic cells. *Environ. Sci. Technol.* **2006**, *40*, 2442–2447. [[CrossRef](#)]

36. Nakada, N.; Tanishima, T.; Shinohara, H.; Kiri, K.; Takada, H. Pharmaceutical chemicals and endocrine disrupters in municipal wastewater in Tokyo and their removal during activated sludge treatment. *Water Res.* **2006**, *40*, 3297–3303. [[CrossRef](#)] [[PubMed](#)]
37. Lee, H.B.; Peart, T.E.; Svoboda, M.L. Determination of ofloxacin, norfloxacin, and ciprofloxacin in sewage by selective solid-phase extraction, liquid chromatography with fluorescence detection, and liquid chromatography-tandem mass spectrometry. *J. Chromatogr. A* **2007**, *1139*, 45–52. [[CrossRef](#)]
38. Jiang, W.T.; Chang, P.H.; Wang, Y.S.; Tsai, Y.; Jean, J.S.; Li, Z.; Krukowski, K. Removal of ciprofloxacin from water by birnessite. *J. Hazard. Mater.* **2013**, *250–251*, 362–369. [[CrossRef](#)]
39. Khan, S.J.; Wang, L.; Hashim, N.H.; McDonald, J.A. Distinct enantiomeric signals of ibuprofen and naproxen in treated wastewater and sewer overflow. *Chirality* **2014**, *26*, 739–746. [[CrossRef](#)]
40. Lishman, L.; Smyth, S.A.; Sarafin, K.; Kleywegt, S.; Toito, J.; Peart, T.; Lee, B.; Servos, M.; Beland, M.; Seto, P. Occurrence and reductions of pharmaceuticals and personal care products and estrogens by municipal wastewater treatment plants in Ontario, Canada. *Sci. Total Environ.* **2006**, *367*, 544–558. [[CrossRef](#)]
41. Khalil, A.M.E.; Memon, F.A.; Tabish, T.A.; Fenton, B.; Salmon, D.; Zhang, S.; Butler, D. Performance evaluation of porous graphene as filter media for the removal of pharmaceutical/emerging contaminants from water and wastewater. *Nanomaterials* **2021**, *11*, 79. [[CrossRef](#)]
42. Han, L.; Khalil, A.M.E.; Wang, J.; Chen, Y.; Li, F.; Chang, H.; Zhang, H.; Liu, X.; Li, G.; Jia, Q.; et al. Graphene-boron nitride composite aerogel: A high efficiency adsorbent for ciprofloxacin removal from water. *Sep. Purif. Technol.* **2022**, *278*, 119605. [[CrossRef](#)]
43. Ismail, Z. Green reduction of graphene oxide by plant extracts: A short review. *Ceram. Int.* **2019**, *45*, 23857–23868. [[CrossRef](#)]
44. Fonseca, A.M.; Monte, F.J.Q.; de Oliveira, M.d.C.F.; de Mattos, M.C.; Cordell, G.A.; Braz-Filho, R.; Lemos, T.L.G. Coconut water (*Cocos nucifera* L.)—A new biocatalyst system for organic synthesis. *J. Mol. Catal. B Enzym.* **2009**, *57*, 78–82. [[CrossRef](#)]
45. Gao, M.; Li, X.; Qi, D.; Lin, J. Green Synthesis of Porous Spherical Reduced Graphene Oxide and Its Application in Immobilized Pectinase. *ACS Omega* **2020**, *5*, 32706–32714. [[CrossRef](#)] [[PubMed](#)]
46. Kurt, B.Z.; Durmus, Z.; Sevgi, E. In situ reduction of graphene oxide by different plant extracts as a green catalyst for selective hydrogenation of nitroarenes. *Int. J. Hydrogen Energy* **2019**, *44*, 26322–26337. [[CrossRef](#)]
47. Joshi, B.; Khalil, A.M.E.; Tabish, T.A.; Memon, F.A.; Chang, H.; Zhang, S. Near Green Synthesis of Porous Graphene from Graphite Using an Encapsulated Ferrate(VI) Oxidant. *ACS Omega* **2023**, *8*, 29674–29684. [[CrossRef](#)]
48. Maamoun, I.; Eljamal, R.; Falyouna, O.; Bensaida, K.; Sugihara, Y.; Eljamal, O. Insights into kinetics, isotherms and thermodynamics of phosphorus sorption onto nanoscale zero-valent iron. *J. Mol. Liq.* **2021**, *328*, 115402. [[CrossRef](#)]
49. Taguba, M.A.M.; Ong, D.C.; Ensano, B.M.B.; Kan, C.C.; Grisdanurak, N.; Yee, J.J.; de Luna, M.D.G. Nonlinear isotherm and kinetic modeling of Cu(II) and Pb(II) uptake from water by MnFe₂O₄/chitosan nano-adsorbents. *Water* **2021**, *13*, 1662. [[CrossRef](#)]
50. Akaike, H. A new look at the statistical model identification. *IEEE Trans. Autom. Control* **1974**, *19*, 716–723. [[CrossRef](#)]
51. Pu, C.; Wan, J.; Liu, E.; Yin, Y.; Li, J.; Ma, Y.; Fan, J.; Hu, X. Two-dimensional porous architecture of protonated GCN and reduced graphene oxide via electrostatic self-assembly strategy for high photocatalytic hydrogen evolution under visible light. *Appl. Surf. Sci.* **2017**, *399*, 139–150. [[CrossRef](#)]
52. Jiang, D.; Chen, L.; Zhu, J.; Chen, M.; Shi, W.; Xie, J. Novel p–n heterojunction photocatalyst constructed by porous graphite-like C₃N₄ and nanostructured BiOI: Facile synthesis and enhanced photocatalytic activity. *J. Chem. Soc. Dalton Trans.* **2013**, *42*, 15726–15734. [[CrossRef](#)]
53. Zhong, Y.; Yuan, J.; Wen, J.; Li, X.; Xu, Y.; Liu, W.; Zhang, S.; Fang, Y. Earth-abundant NiS co-catalyst modified metal-free mpg-C₃N₄/CNT nanocomposites for highly efficient visible-light photocatalytic H₂ evolution. *Dalton Trans.* **2015**, *44*, 18260–18269. [[CrossRef](#)] [[PubMed](#)]
54. Guo, F.; Creighton, M.; Chen, Y.; Hurt, R.; Külaots, I. Porous structures in stacked, crumpled and pillared graphene-based 3D materials. *Carbon* **2014**, *66*, 476–484. [[CrossRef](#)] [[PubMed](#)]
55. Cai, N.; Larese-Casanova, P. Sorption of carbamazepine by commercial graphene oxides: A comparative study with granular activated carbon and multiwalled carbon nanotubes. *J. Colloid Interface Sci.* **2014**, *426*, 152–161. [[CrossRef](#)] [[PubMed](#)]
56. Putra, A.; Masriati, S.; Amran, A. The Association Structures and Sustainability of Methyl Red and Methylene Blue In Water Systems, A Nonionic Surfactants (Tween-40 And Tween-80) And Cyclohexane. *Int. J. Progress. Sci. Technol.* **2019**, *17*, 117–125.
57. Mottram, L.F.; Forbes, S.; Ackley, B.D.; Peterson, B.R. Hydrophobic analogues of rhodamine B and rhodamine 101: Potent fluorescent probes of mitochondria in living *C. elegans*. *Beilstein J. Org. Chem.* **2012**, *8*, 2156–2165. [[CrossRef](#)]
58. Yakimova, L.S.; Shurpik, D.N.; Gilmanova, L.H.; Makhmutova, A.R.; Rakhimbekova, A.; Stoikov, I.I. Highly selective binding of methyl orange dye by cationic water-soluble pillar[5]arenes. *Org. Biomol. Chem.* **2016**, *14*, 4233–4238. [[CrossRef](#)]
59. Thomas, S.; Shanks, R.; Chandran, S. (Eds.) *Design and Applications of Nanostructured Polymer Blends and Nanocomposite Systems*; William Andrew: Norwich, NY, USA, 2015.
60. Chao, Y.; Zhu, W.; Wu, X.; Hou, F.; Xun, S.; Wu, P.; Ji, H.; Xu, H.; Li, H. Application of graphene-like layered molybdenum disulfide and its excellent adsorption behavior for doxycycline antibiotic. *Chem. Eng. J.* **2014**, *243*, 60–67. [[CrossRef](#)]
61. Perwitasari, D.S.; Ardian, Y.; Pracesa, Y.; Pangestu, M.A.; Sampe Tola, P. Langmuir and Freundlich Isotherm Approximation on Adsorption Mechanism of Chrome Waste by Using Tofu Dregs. *Nusant. Sci. Technol. Proc.* **2021**, 106–112. [[CrossRef](#)]
62. Dada, A.O.; Olalekan. Langmuir, Freundlich, Temkin and Dubinin–Radushkevich Isotherms Studies of Equilibrium Sorption of Zn²⁺ Unto Phosphoric Acid Modified Rice Husk. *IOSR J. Appl. Chem.* **2012**, *3*, 38–45. [[CrossRef](#)]

63. Waheed, A.; Baig, N.; Ullah, N.; Falath, W. Removal of hazardous dyes, toxic metal ions and organic pollutants from wastewater by using porous hyper-cross-linked polymeric materials: A review of recent advances. *J. Environ. Manag.* **2021**, *287*, 112360. [[CrossRef](#)]
64. Ji, L.; Chen, W.; Bi, J.; Zheng, S.; Xu, Z.; Zhu, D.; Alvarez, P.J. Adsorption of tetracycline on single-walled and multi-walled carbon nanotubes as affected by aqueous solution chemistry. *Environ. Toxicol. Chem.* **2010**, *29*, 2713–2719. [[CrossRef](#)]
65. Chiang, C.H.; Chen, J.; Lin, J.H. Preparation of pore-size tunable activated carbon derived from waste coffee grounds for high adsorption capacities of organic dyes. *J. Environ. Chem. Eng.* **2020**, *8*, 103929. [[CrossRef](#)]
66. Liu, F.F.; Zhao, J.; Wang, S.; Du, P.; Xing, B. Effects of solution chemistry on adsorption of selected pharmaceuticals and personal care products (PPCPs) by graphenes and carbon nanotubes. *Environ. Sci. Technol.* **2014**, *48*, 13197–13206. [[CrossRef](#)] [[PubMed](#)]
67. Marchesini, S.; Turner, P.; Paton, K.R.; Reed, B.P.; Brennan, B.; Koziol, K.; Pollard, A.J. Gas physisorption measurements as a quality control tool for the properties of graphene/graphite powders. *Carbon* **2020**, *167*, 585–595. [[CrossRef](#)]
68. Igwegbe, C.A.; Oba, S.N.; Aniagor, C.O.; Adeniyi, A.G.; Ighalo, J.O. Adsorption of ciprofloxacin from water: A comprehensive review. *J. Ind. Eng. Chem.* **2021**, *93*, 57–77. [[CrossRef](#)]
69. Cai, N.; Larese-Casanova, P. Application of positively-charged ethylenediamine-functionalized graphene for the sorption of anionic organic contaminants from water. *J. Environ. Chem. Eng.* **2016**, *4*, 2941–2951. [[CrossRef](#)]
70. Robati, D.; Mirza, B.; Rajabi, M.; Moradi, O.; Tyagi, I.; Agarwal, S.; Gupta, V.K. Removal of hazardous dyes-BR 12 and methyl orange using graphene oxide as an adsorbent from aqueous phase. *Chem. Eng. J.* **2016**, *284*, 687–697. [[CrossRef](#)]
71. Ramesha, G.K.; Kumara, A.V.; Muralidhara, H.B.; Sampath, S. Graphene and graphene oxide as effective adsorbents toward anionic and cationic dyes. *J. Colloid Interface Sci.* **2011**, *361*, 270–277. [[CrossRef](#)]
72. Dong, Q.; Wang, G.; Qian, B.; Hu, C.; Wang, Y.; Qiu, J. Electrospun composites made of reduced graphene oxide and activated carbon nanofibers for capacitive deionization. *Electrochim. Acta* **2014**, *137*, 388–394. [[CrossRef](#)]
73. Zaka, A.; Ibrahim, T.H.; Khamis, M.I.; Samara, F. Adsorption characteristics of diclofenac sodium onto graphene nanoplatelets. *Desalination Water Treat.* **2020**, *206*, 331–339. [[CrossRef](#)]
74. Malakootian, M.; Faraji, M.; Malakootian, M.; Nozari, M. Ciprofloxacin removal from aqueous media by adsorption process: A systematic review and meta-analysis. *Desalination Water Treat.* **2021**, *229*, 252–282. [[CrossRef](#)]
75. Rout, D.R.; Jena, H.M. Removal of malachite green dye from aqueous solution using reduced graphene oxide as an adsorbent. *Mater. Today Proc.* **2021**, *47*, 1173–1182. [[CrossRef](#)]
76. Floare-Avram, C.V.; Marincas, O.; Feher, I.; Covaciu, F.D.; Floare, C.G.; Lazar, M.D.; Magdas, D.A. Characterization of the Adsorption of Bisphenol A and Carbamazepine from Aqueous Solution on Graphene Oxide and Partially Reduced Graphene Oxide by High-Performance Liquid Chromatography (HPLC). *Anal. Lett.* **2023**, *56*, 272–285. [[CrossRef](#)]
77. Minitha, C.R.; Lalitha, M.; Jeyachandran, Y.L.; Senthilkumar, L.; Rajendra Kumar, R.T. Adsorption behaviour of reduced graphene oxide towards cationic and anionic dyes: Co-action of electrostatic and π - π interactions. *Mater. Chem. Phys.* **2017**, *194*, 243–252. [[CrossRef](#)]
78. Tan, K.B.; Vakili, M.; Horri, B.A.; Poh, P.E.; Abdullah, A.Z.; Salamatinia, B. Adsorption of dyes by nanomaterials: Recent developments and adsorption mechanisms. *Sep. Purif. Technol.* **2015**, *150*, 229–242. [[CrossRef](#)]
79. Yao, Y.; Bing, H.; Feifei, X.; Xiaofeng, C. Equilibrium and kinetic studies of methyl orange adsorption on multiwalled carbon nanotubes. *Chem. Eng. J.* **2011**, *170*, 82–89. [[CrossRef](#)]
80. Yu, Z.; Peldszus, S.; Huck, P.M. Adsorption characteristics of selected pharmaceuticals and an endocrine disrupting compound-Naproxen, carbamazepine and nonylphenol-on activated carbon. *Water Res.* **2008**, *42*, 2873–2882. [[CrossRef](#)]
81. Pal, J.; Deb, M.K.; Deshmukh, D.K.; Verma, D. Removal of methyl orange by activated carbon modified by silver nanoparticles. *Appl. Water Sci.* **2013**, *3*, 367–374. [[CrossRef](#)]
82. Baccar, R.; Sarrà, M.; Bouzid, J.; Feki, M.; Blázquez, P. Removal of pharmaceutical compounds by activated carbon prepared from agricultural by-product. *Chem. Eng. J.* **2012**, *211–212*, 310–317. [[CrossRef](#)]

Disclaimer/Publisher’s Note: The statements, opinions and data contained in all publications are solely those of the individual author(s) and contributor(s) and not of MDPI and/or the editor(s). MDPI and/or the editor(s) disclaim responsibility for any injury to people or property resulting from any ideas, methods, instructions or products referred to in the content.